J. Fluid Mech. (1982), *vol.* 122, *pp.* 1–12
Printed in Great Britain

Buoyancy-driven circulation in free-surface channels

By SUBHASH C. JAIN
Iowa Institute of Hydraulic Research, The University of Iowa, Iowa City, Iowa 52242

(Received 18 September 1981 and in revised form 15 March 1982)

The convective circulation driven by a surface buoyancy flux in a dead-end open channel is analysed. On the assumption of similarity profiles for velocity and temperature, the governing partial differential are reduced to two nonlinear ordinary differential equations by integrating over the flow depth. A closed-form solution of the differential equations is presented. The solution is a function of the Grashof number G and the modified Prandtl–Grashof number $P_m G^{\frac{1}{4}}$ defined in (21). The velocity and temperature along the channel vary linearly as the distance and as the square of the distance respectively. Analytical expressions for the rate of total heat loss from the channel and the rate of flow in the channel are derived. The analytical results compare well with the available experimental data.

1. Introduction

The convective circulation considered in this paper occurs in sidearms (dead-end channels) of cooling lakes used for the disposal of water heat from electric power generation. These dead end channels are very effective in heat dissipation to the atmosphere owing to strong density currents developed in them (Ryan, Harleman & Stolzenbach 1974). The physical processes that are responsible for the development of the convective circulation in dead-end channels are explained by Sturm & Kennedy (1980), and are summarized as follows. The warmer and lighter water from the main lake spread as a surface layer into the dead-end channel, as shown in figure 1. There is a continuous surface buoyancy flux B from the upper layer into the atmosphere by the surface cooling; consequently the temperature of the upper layer decreases and the density of water in the upper layer increases along the x-direction. There develops a positive longitudinal density gradient along the x-direction which drives the bottom current from the channel into the main reservoir.

The flow field in a dead end channel is similar to that in the Red Sea described by Phillips (1966). The surface buoyancy flux in the Red Sea is the result of the surface cooling and the increase of salinity due to evaporation. Using dimensional reasoning, Phillips presented a similarity solution for a constant surface buoyancy flux. The present author (Jain 1980) extended Phillips' similarity solution to a case where the surface buoyancy flux is linearly proportional to the water surface temperature. Both Phillips' and the author's analyses showed that the longitudinal velocity decays along the x-direction; consequently there is continuous downflow from the upper layer into the lower layer. Brocard & Harleman (1980) observed such a downflow in some of their laboratory experiments on convective circulation. The absence of the sharp gradients in the measured vertical buoyancy profiles for the Red Sea presented by

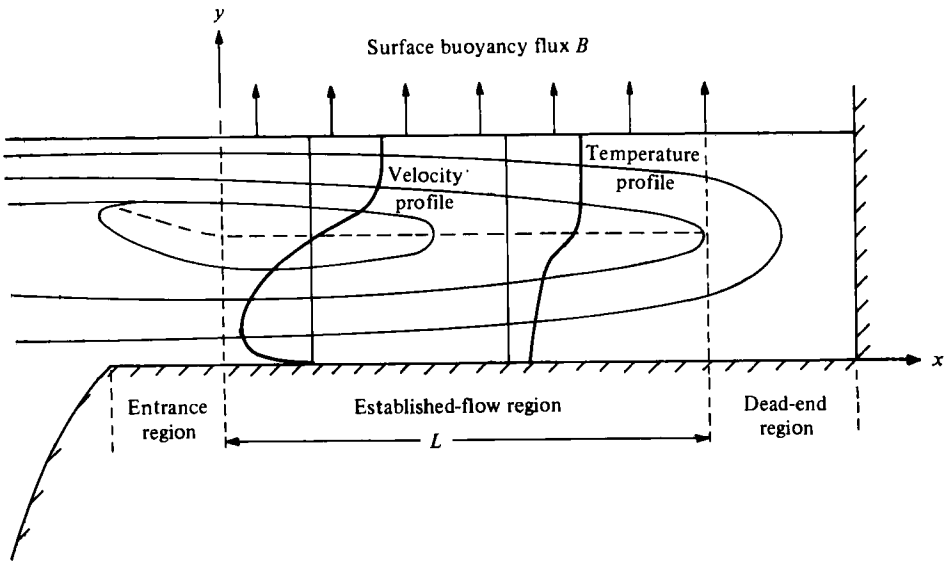

FIGURE 1. Convective circulation in free-surface channel.

Phillips corroborates the hypothesis of the continuous downflow. This continuous downflow is the result of convective motions in the unstable upper layer due to surface cooling penetrating into the lower stable layer. The two-layer model for convective circulation presented by Brocard & Harleman (1980) does not consider the continuous downflow, and is therefore applicable to short channels where the downflow can be neglected. Sturm & Kennedy (1980) solved the governing equations numerically for the convective flow in a dead-end channel and presented the correlation of the numerical results to allow an estimate of heat loss from the sidearm. An exact analytical solution of the governing equations is presented in this paper. The solution is based on the similarity assumption, which leads to a continuous distribution of downflow.

2. Analytical model

The flow field in the channel is divided into three regions: the entrance region, the established-flow region and the dead-end region. The entrance region, which is a few depths in length, is characterized by rapid changes in velocity and temperature along the streamwise direction and in the elevation of the interface between the two layers. For the shallow upper layer at the entrance, the inflow of warm water into the channel acts like a buoyant surface jet. The thickness of the upper layer increases rapidly owing to entrainment in the entrance region, and approaches an equilibrium value at the end of the entrance region. For deeper entrance upper-layer depths, the thickness of the upper layer decreases rapidly to a final equilibrium value. In the established-flow region the velocity and temperature gradients along the x-direction are much smaller than those along the y-direction, and the interface elevation is practically constant. The flow field in this region is governed primarily by the surface buoyancy flux and the viscous forces. The surface buoyancy flux B is due to the surface cooling, and is given by

$$B = \beta g \Phi / \rho C_p, \tag{1}$$

where g is the gravitational acceleration, $\beta = (-1/\rho)\,\partial\rho/\partial T$ is the thermal coefficient of the water, Φ is the surface heat flux per unit surface area, and C_p, ρ and T are respectively the specific heat, density and temperature of the water. The surface heat flux, which is a function of the water-surface temperature T_s and the meteorological conditions, is determined from a linearized relation introduced by Edinger & Geyer (1965):

$$\Phi = K(T_s - T_e), \tag{2}$$

where K is the surface heat-exchange coefficient and T_e is the equilibrium temperature. Φ in (2) is counted positively upward along the y-direction. In the established-flow region the flow rate and temperature of the upper layer decreases continuously, as explained in § 1. If the channel is sufficiently long, the water surface temperature at a certain distance L_e from the beginning of the established region ($x = 0$) will cool down to the equilibrium temperature, and the channel beyond this section will not be effective in cooling. The flow velocity at this section, as shown in § 2.4, is zero. The length L_e is hereinafter referred to as the equilibrium length. Channels of length $L \geqslant L_e$ and $L < L_e$ are hereinafter referred to as long and short channels respectively. For a dead-end short channel the flow in the upper layer near the dead end of the channel is non-zero. The region of downflow near the dead end of the short channel is called a dead-end region.

2.1. *Governing equations and boundary conditions*

The analysis presented in this paper is concerned with the established region of channels of uniform width and with horizontal bottoms. Lateral uniformity is assumed, leading to a two-dimensional problem in the vertical plane. The governing equations for the flow in the established region, where the vertical velocity and temperature gradients are much greater than the corresponding horizontal gradients (boundary-layer approximations), and where the effect of density variation is important only on the buoyancy term (Boussinesq's approximation), are:

$$\frac{\partial u}{\partial x} + \frac{\partial v}{\partial y} = 0 \quad \text{(continuity)}, \tag{3}$$

$$u\frac{\partial u}{\partial x} + v\frac{\partial u}{\partial y} = -\frac{1}{\rho_e}\frac{\partial p}{\partial x} + \frac{1}{\rho_e}\frac{\partial \tau_{xy}}{\partial y} \quad (x\text{-momentum}), \tag{4}$$

$$0 = -\frac{\partial p}{\partial y} - \rho g \quad (y\text{-momentum}), \tag{5}$$

$$u\frac{\partial T}{\partial x} + v\frac{\partial T}{\partial y} = \frac{\partial}{\partial y}\left(D_y\frac{\partial T}{\partial y}\right) \quad \text{(thermal energy)}, \tag{6}$$

$$\rho = -\beta\rho_e T + \alpha \quad \text{(state)}, \tag{7}$$

where u and v are the components of time-averaged velocity vectors along the x- and y-directions respectively, p is the pressure, T is the time-averaged temperature, ρ_e is the water density at the equilibrium temperature, α is a constant, τ_{xy} is the shear stress, and D_y is the thermal diffusivity. Elimination of the pressure term between

(4) and (5), and integration of the continuity, momentum and energy equations over the flow depth D, reduces them to

$$\int_0^{D(x)} u\,dy = 0, \tag{8}$$

$$\frac{d}{dx}\int_0^{D(x)} u^2\,dy = -\frac{g}{\rho_e}\frac{d}{dx}\int_0^{D(x)}\int_y^{D(x)} (-\beta\rho_e T+\alpha)\,dy\,dy - \frac{\tau_0}{\rho_e}, \tag{9}$$

$$\frac{d}{dx}\int_0^{D(x)} uT\,dy = D_y\frac{\partial T}{\partial y}\bigg|_{y=D(x)} \equiv -\frac{\Phi(T_s)}{\rho_e C_p}, \tag{10}$$

where τ_0 is the shear stress at the channel bottom. Equations (9) and (10) are reduced to ordinary differential equations by invoking the following assumptions. It was observed in the laboratory experiments reported by Brocard, Jirka & Harleman (1977) and Sturm (1976) that the water surface and the interface deviations were almost constant in the channel, and that the flow in the lower layer was laminar. The effect of the water-surface slope is therefore neglected. The bottom shear stress in (9) is expressed as

$$\frac{\tau_0}{\rho_e} = \nu\left(\frac{\partial u}{\partial y}\right)\bigg|_{y=0}, \tag{11}$$

where ν is the kinematic viscosity of the fluid. The vertical velocity and temperature profiles are assumed to be similar, and are denoted by

$$f(\eta) = \frac{u}{u_s}, \tag{12}$$

$$h(\eta) = \frac{T-T_n}{T_s-T_n}, \tag{13}$$

where u_s is the flow velocity at the water surface, T_s is the water-surface temperature, T_n is the temperature at the end of the established region, and $\eta = y/D$. The integrated momentum and energy equations (9) and (10), upon substitution for Φ, u, T and τ_0 from (2), (11), (12) and (13), and integration reduce to

$$2C_1 D u_s\frac{du_s}{dx} - C_2\beta g D^2\frac{d}{dx}(T_s-T_n) - C_3\frac{\nu}{D}u_s = 0, \tag{14}$$

$$C_4 D\frac{d}{dx}[u_s(T_s-T_n)] + k(T_s-T_e) = 0, \tag{15}$$

where the constants C_1, through C_4 result from the integration of the various products of $f(\eta)$ and $h(\eta)$:

$$C_1 = \int_0^1 f^2(\eta)\,d\eta, \quad C_2 = \int_0^1\int_\eta^1 h(\eta)\,d\eta\,d\eta,$$

$$C_3 = -f'(\eta)\big|_{\eta=0}, \quad C_4 = \int_0^1 f(\eta)h(\eta)\,d\eta, \quad k = K/\rho_e C_p.$$

In a buoyancy driven flow, there is no characteristic velocity independent of the flow. The boundary conditions for the two ordinary differential equations (14) and (15) are therefore expressed in terms of temperatures at the two ends of the established region, i.e.

$$T_s = T_0 \quad (x=0), \quad T_s = T_n \quad (x=L), \tag{16}$$

where T_0 is the water-surface temperature at the beginning of the established region. T_n in (16) is an unknown. Since there is no independent velocity in such flows, the velocity in (14) and (15) is normalized by $[\beta(T_0-T_e)gD]^{\frac{1}{2}}$, which is the surface spreading rate of a buoyant layer. The temperatures in (14) and (15) are normalized by T_0-T_e. Equations (14) and (15) on normalization reduce to

$$\phi\phi'-\gamma_1\theta'-\gamma_2\phi=0, \tag{17}$$

$$\theta\phi'+\theta'\phi+\gamma_3(\theta+\theta_n)=0, \tag{18}$$

where

$$\phi=\frac{u_s}{[\beta(T_0-T_e)gD]^{\frac{1}{2}}},\quad \theta=\frac{T_s-T_n}{T_0-T_e},\quad \theta_n=\frac{T_n-T_e}{T_0-T_e}, \tag{19}$$

$$\gamma_1=\frac{C_2}{2C_1},\quad \gamma_2=\frac{C_3}{2C_1}\frac{1}{G^{\frac{1}{2}}},\quad \gamma_3=\frac{1}{C_4P_mG^{\frac{1}{2}}}. \tag{20}$$

$$G=\frac{\beta(T_0-T_e)gD^3}{\nu^2},\quad P_mG^{\frac{1}{2}}=\frac{[\beta(T_0-T_e)gD]^{\frac{1}{2}}}{k}. \tag{21}$$

The primes in (17) and (18) denotes differentiation with respect to $\xi=x/D$. It should be noted that the coefficients γ_1, γ_2 and γ_3 in (17) and (18) are positive. The normalized equations (17) and (18) contain two dimensionless governing parameters: the Grashof number G and the modified Prandtl–Grashof number $P_mG^{\frac{1}{2}}$. The Grashof number represents the ratio of the buoyancy to viscous forces. The modified Prandtl–Grashof number, as shown in §2.4, is the ratio of the surface spreading rate of a buoyant layer to the sinking rate of the water from the upper layer into the lower layer. The boundary conditions given by (16) reduce in the normalized form to

$$\theta=1-\theta_n\quad(\xi=0),\quad \theta=0\quad(\xi=L^0), \tag{22}$$

where $L^0=L/D$.

2.2. *Analytical solution*

The differential equations (17) and (18) do not contain the independent variable ξ explicitly. This system of nonlinear ordinary differential equations can be reduced to an equation of first order in ϕ and θ. On eliminating ϕ' from (17) and (18) one gets

$$\theta'=-[(\gamma_2+\gamma_3)\theta\phi+\gamma_3\theta_n\phi]/(\phi^2+\gamma_1\theta). \tag{23}$$

Similarly the elimination of θ' from (17) and (18) yields

$$\phi'=[\gamma_2\phi^2-\gamma_1\gamma_3(\theta+\theta_n)]/(\phi^2+\gamma_1\theta). \tag{24}$$

If (24) is divided by (23), the following equation of first order is obtained:

$$\frac{d\phi}{d\theta}+f(\theta)\phi=g(\theta)\phi^n, \tag{25}$$

where

$$\left.\begin{aligned} f(\theta)&=\gamma_2/[(\gamma_2+\gamma_3)\theta+\gamma_3\theta_n],\\ g(\theta)&=\gamma_1\gamma_3(\theta+\theta_n)/[(\gamma_2+\gamma_3)\theta+\gamma_3\theta_n],\\ n&=-1. \end{aligned}\right\} \tag{26}$$

Equation (25) is the Bernoulli equation (Ames 1968), which can be solved using the transformation

$$\phi=u^{1/(1-n)}. \tag{27}$$

With this transformation (25) takes the form

$$\frac{du}{d\theta}+(1-n)f(\theta)\,u=(1-n)\,g(\theta), \tag{28}$$

whose solution is

$$u=\exp\left[(n-1)\int f(\theta)\,d\theta\right]\{A-(n-1)\int g(\theta)\left[(1-n)\int f(\theta)\,d\theta\right]d\theta\}, \tag{29}$$

where A is a constant of integration. On substituting for $f(\theta)$, $g(\theta)$ and n from (26) into (29) and integrating, one obtains

$$u=\frac{A}{\psi^{2\gamma_2/(\gamma_2+\gamma_3)}}+\frac{2\gamma_1\gamma_3\psi}{(\gamma_2+\gamma_3)(3\gamma_2+\gamma_3)}+\frac{\gamma_1\gamma_3\theta_n}{(\gamma_2+\gamma_3)}, \tag{30}$$

where

$$\psi=(\gamma_2+\gamma_3)\,\theta+\gamma_3\theta_n. \tag{31}$$

The constant A must be put equal to zero, since the velocity must remain finite when ψ goes to zero. Thus the solution of (25) from (27) and (30) is

$$\phi^2=(\theta+\tfrac{3}{2}\theta_n)/\delta_1, \tag{32}$$

where

$$\delta_1=(3\gamma_2+\gamma_3)/2\gamma_1\gamma_3. \tag{33}$$

On substituting for ϕ from (32) into (24), and simplifying, one obtains

$$d\phi/d\xi=-\tfrac{1}{3}\gamma_3, \tag{34}$$

which on integration yields

$$\phi=-\tfrac{1}{3}\gamma_3\xi+B, \tag{35}$$

where B is a constant of integration. The value of the constant of integration B is obtained by substituting for ϕ from (32) into (35) and using the boundary condition $\theta=1-\theta_n$ at $\xi=0$ from (22):

$$B=[(1+\tfrac{1}{2}\theta_n)/\delta_1]^{\frac{1}{2}}.$$

Hence the solution of the governing equations (17) and (18) is

$$\phi=\left[\frac{1+\tfrac{1}{2}\theta_n}{\delta_1}\right]^{\frac{1}{2}}-\tfrac{1}{3}\gamma_3\xi, \tag{36}$$

$$\theta=\delta_1\left\{\left[\frac{1+\tfrac{1}{2}\theta_n}{\delta_1}\right]^{\frac{1}{2}}-\tfrac{1}{3}\gamma_3\xi\right\}^2-\tfrac{3}{2}\theta_n. \tag{37}$$

The unknown θ_n is determined from the boundary condition $\theta=0$ at $\xi=L^0$ from (22):

$$\theta_n=(1+\tfrac{2}{9}\gamma_3^2L^{0^2}\delta_1)-(\tfrac{2}{3}\gamma_3^2L^{0^2}\delta_1+\tfrac{1}{27}\gamma_3^4L^{0^4}\delta_1^2)^{\frac{1}{2}}. \tag{38}$$

An expression for the equilibrium length L_e for a channel, as defined earlier, is obtained on substituting $\theta_n=0$ in (38), and is given by

$$L_e^0=3/\gamma_3\delta_1^{\frac{1}{2}}, \tag{39}$$

where $L_e^0=L_e/D$.

2.3. *Analytical results*

A summary of the analytical solution is given below:

$$\theta=[(1+\tfrac{1}{2}\theta_n)^{\frac{1}{2}}-x/L_e]^2-\tfrac{3}{2}\theta_n, \tag{40}$$

$$\phi_\delta=(1+\tfrac{1}{2}\theta_n)^{\frac{1}{2}}-x/L_e, \tag{41}$$

where
$$\theta_n = 1 + 2\lambda^2 - (6\lambda^2 + 3\lambda^4)^{\frac{1}{2}}, \tag{42}$$

$$L_e^0 = \left\{\frac{18 C_2 C_4^2}{2C_1/(P_m G^{\frac{1}{2}})^2 + 3C_3 C_4/P_m G^{\frac{1}{2}} G^{\frac{1}{2}}}\right\}^{\frac{1}{2}}, \tag{43}$$

$$\lambda = L/L_e, \quad \phi_\delta = \phi \delta_1^{\frac{1}{2}}, \tag{44}$$

$$\delta_1 = \frac{2C_1 + 3C_3 C_4 P_m}{2C_2}. \tag{45}$$

The expressions for the rate of total surface heat loss from, and the rate of flow into, the upper layer of the channel are of practical interest in evaluating the cooling potential of a lake on the waste-heat loading from a power plant. The rate of surface heat loss H_L from a unit width of a channel of length L is

$$H_L = \int_0^L K(T_s - T_e)\, dx, \tag{46}$$

which on substituting for T_s from (40), and on integrating reduces to

$$H_L = KL_e(T_0 - T_e)\{\lambda + \tfrac{1}{3}\lambda^3 - \lambda^2[\tfrac{3}{2} + \lambda^2 - (\tfrac{3}{2}\lambda^2 + \tfrac{3}{4}\lambda^4)^{\frac{1}{2}}]^{\frac{1}{2}}\}. \tag{47}$$

The rate of total surface heat loss H_{Le} from unit width of a long channel is obtained by substituting unity for λ in (47):

$$H_{Le} = \tfrac{1}{3} KL_e(T_0 - T_e). \tag{48}$$

The ratio η_H of total heat loss from a short channel of length L to that from a long channel from (47) and (48) is a function of λ only, and is given by

$$\eta_H = 3\lambda\{1 + \tfrac{1}{3}\lambda^2 - \lambda[\tfrac{3}{2} + \lambda^2 - (\tfrac{3}{2}\lambda^2 + \tfrac{3}{4}\lambda^4)^{\frac{1}{2}}]^{\frac{1}{2}}\}. \tag{49}$$

The surface velocity as determined from (41) is

$$\frac{u_s}{kL_0^0} = \frac{(1 + \frac{1}{2}\theta_n)^{\frac{1}{2}} - x/L_e}{3C_4}, \tag{50}$$

and the flow rate q per unit channel width in the upper layer is obtained by integrating the velocity distribution over the upper layer depth and substituting for u_s from (50):

$$\frac{q}{kL_e} = \frac{C_5}{3C_4}\left[(1 + \tfrac{1}{2}\theta_n)^{\frac{1}{2}} - \frac{x}{L_e}\right], \tag{51}$$

where $C_5 = \int_\Lambda^1 f(\eta)\, d\eta$ and $f(\Lambda) = 0$. θ_n in (50) and (51) can be expressed in terms of λ from (42). The rate of flow in the upper layer decreases linearly with distance x. The rate V of continuous downflow from the upper layer into the lower layer is, from (51),

$$V = \frac{C_5}{3C_4} k, \tag{52}$$

which shows that the rate of continuous downflow is directly proportional to the surface heat-loss coefficient. The unit flow rate q_0 at $x = 0$ is, from (51),

$$\frac{q_0}{kL_e} = \frac{C_5}{3C_4}(1 + \tfrac{1}{2}\theta_n)^{\frac{1}{2}}. \tag{53}$$

The unit discharge q_{0e} for a long channel is obtained on substituting $\theta_n = 0$ in (53). An expression for the normalized discharge η_{q_0} is

$$\eta_{q_0} \equiv q_0/q_{0e} = [\tfrac{3}{2} + \lambda^2 - (\tfrac{3}{2}\lambda^2 + \tfrac{3}{4}\lambda^4)^{\frac{1}{2}}]^{\frac{1}{2}}. \tag{54}$$

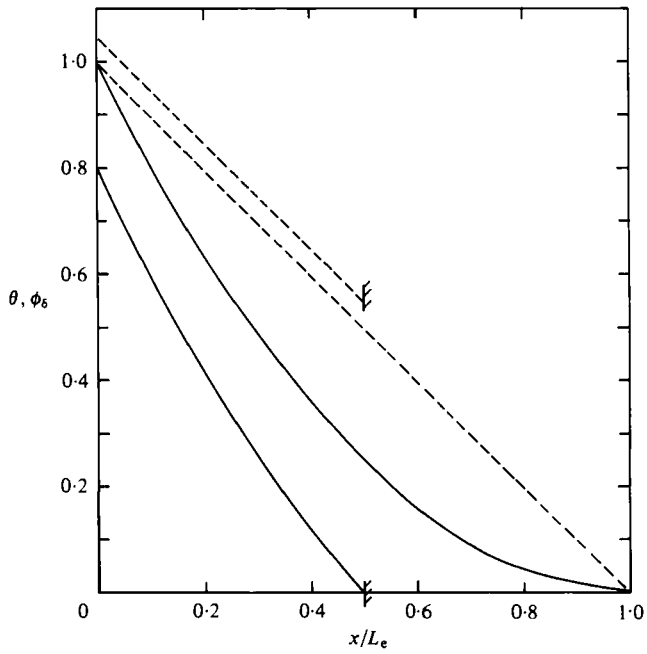

FIGURE 2. Variation of surface temperature and velocity along the channel. ——, θ; – – – –, ϕ_δ.

2.4. *Discussion of analytical results*

Introduction of the equilibrium length L_e made it possible to present the analytical solutions (§2.3) in generalized form. L_e given by (43) is a function of velocity and temperature profiles, the constants $C_1, \ldots, C_4$, and the dimensionless governing parameters $P_m G^{\frac{1}{2}}$ and G. It can be shown from (52) that the parameter $P_m G^{\frac{1}{2}}$ defined in (21) represents the ratio of the surface spreading rate of the buoyant layer to the rate of the continuous downflow from the upper layer into the lower layer. One would expect L_e to increase with the increase in the ratio of either the surface spreading rate of the buoyant layer to the sinking rate of the continuous downflow, i.e. $P_m G^{\frac{1}{2}}$, or the buoyancy force to the viscous force, i.e. G; and indeed that is the case, as can be seen from (43).

The variations of the surface temperature and velocity along the channel for a long channel ($\lambda \geqslant 1$) and a short channel ($\lambda = 0{\cdot}5$) are presented in figure 2. The value of θ_n for $\lambda = 0{\cdot}5$ from (42) is 0·2. The increase in the surface velocity for short channels is due to the reduction in the overall friction larger than that in the overall longitudinal density gradient. Heat conservation for short channels, in which there is an increase in net local flux due to the increase in the surface velocity, is satisfied by the increase in the temperature decay. The velocity at $x = L_e$ is zero; hence a long channel beyond this section is not effective in cooling.

The effect of the channel length on θ_n, η_H, and η_{q_0} from (42), (49) and (54), while the other variables are held constant, is shown in figure 3. The rate of change of θ_n and η_H with λ decreases rapidly with increase in λ. Indeed, about 84% of the maximum surface heat loss and 80% of the maximum surface-temperature drop occur in a

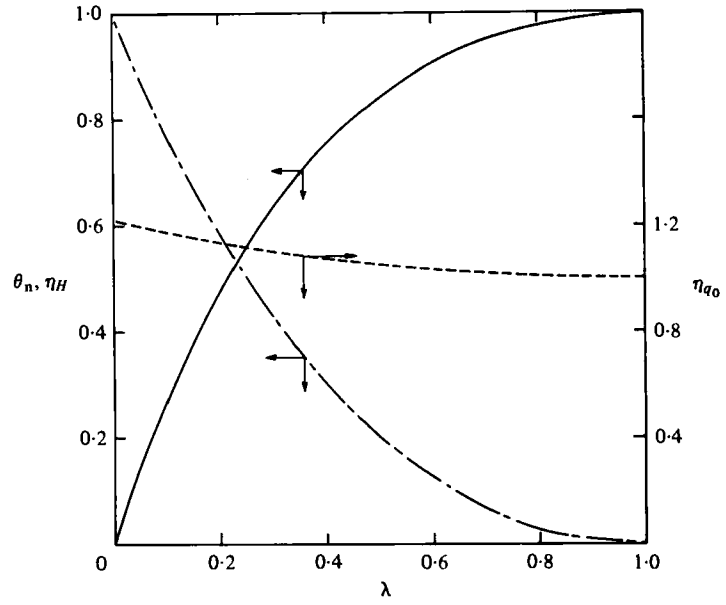

FIGURE 3. Analytical results for dimensionless dead-end temperature, surface heat loss, and discharge: — — —, θ_n; ——, η_H; – – – – –, η_{q_0}.

channel length equal to 50% of the equilibrium length. The unit discharge in the upper layer increases with the decrease in the channel length. The maximum value of η_{q_0} that occurs for $\lambda = 0$ is $\sqrt{\frac{3}{2}}$. The reason for the increase in q_0 for short channels is the same as that for the surface velocity explained earlier.

3. Comparison of analytical and experimental results

The analytical results are compared with the experimental data of Brocard *et al.* (1977). Their experimental set-up was an insulated flume 2·5 ft wide, 1 ft deep, and of adjustable length up to 35 ft, connected to a large rectangular basin. The value of θ_n in their experiments ranged from 0·82 to 0·95, which indicates that the experimental channel was a 'short' channel. It is not possible to compute the profile constants as no detailed measurements of vertical velocity profiles were reported. The experimental runs in which the elevation of the interface did not change significantly along the channel were selected for comparison. The length of the established-flow region was assumed equal to the length of the experimental channel for these selected runs. The values for the equilibrium length L_e of the channel were computed from (42) using the measured values of θ_n.

The surface-temperature distributions along the channel for runs 13 and 14 are compared with (40) in figure 4. The agreement of the experimental data with the analytical solution is fairly good. Since L_e is the most significant parameter in the analytical solution, it is essential to verify (43) using the experimental data. Equation (43) can be written as

$$\lambda = \frac{1}{\delta_2}\left[\frac{k^2L^2}{\beta(T_0 - T_e)gD^3}\right]^{\frac{1}{3}}, \tag{55}$$

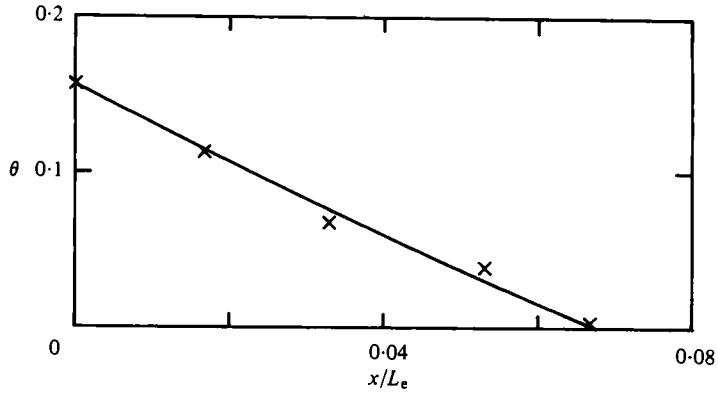

FIGURE 4. Comparison of (40) for longitudinal distribution of surface temperature with the experimental data of Brocard *et al.* (1977). ×, run 14.

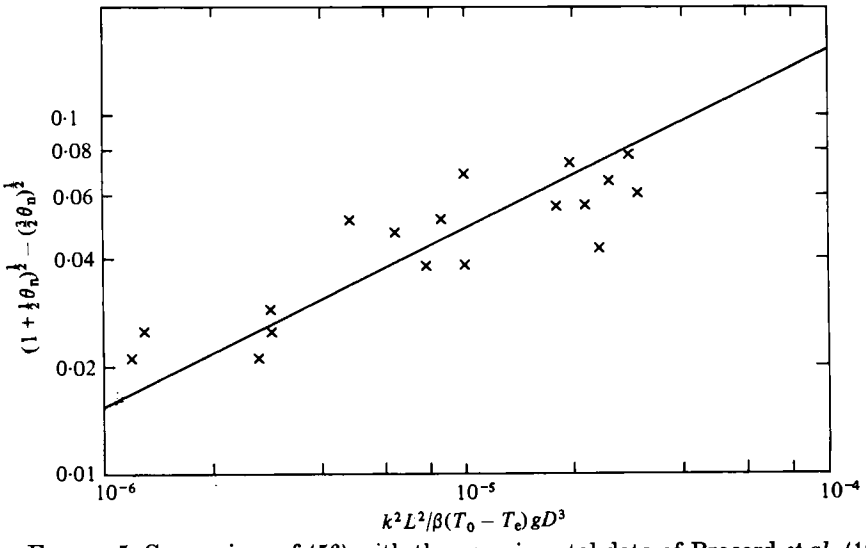

FIGURE 5. Comparison of (56) with the experimental data of Brocard *et al.* (1977).

where $\delta_2 = 3C_4[2C_2/(2C_1+3C_3C_4P_m)]^{\frac{1}{2}}$ is a constant for a constant value of P_m. On equating the value of λ from (40) to that from (55), one gets

$$(1+\tfrac{1}{2}\theta_n)^{\frac{1}{2}} - (\tfrac{3}{2}\theta_n)^{\frac{1}{2}} = \frac{1}{\delta_2}\left[\frac{k^2L^2}{\beta(T_0-T_e)gD^3}\right]^{\frac{1}{2}}. \tag{56}$$

The selected experimental data for which the values of P_m were almost same are compared with (56) in figure 5. The agreement between theory and measurements is satisfactory. Brocard *et al.* (1977) also presented data for the non-dimensional discharge q_0/kL into the channel. Equation (53) on substituting for L_e from (55) reduces to

$$\frac{q_0/kL}{(1+\frac{1}{2}\theta_n)^{\frac{1}{2}}} = \frac{C_5\delta_2}{3C_4}\left[\frac{\beta(T_0-T_e)gD^3}{k^2L^2}\right]^{\frac{1}{2}}. \tag{57}$$

The agreement between (57) and the measurements shown in figure 6 is considered

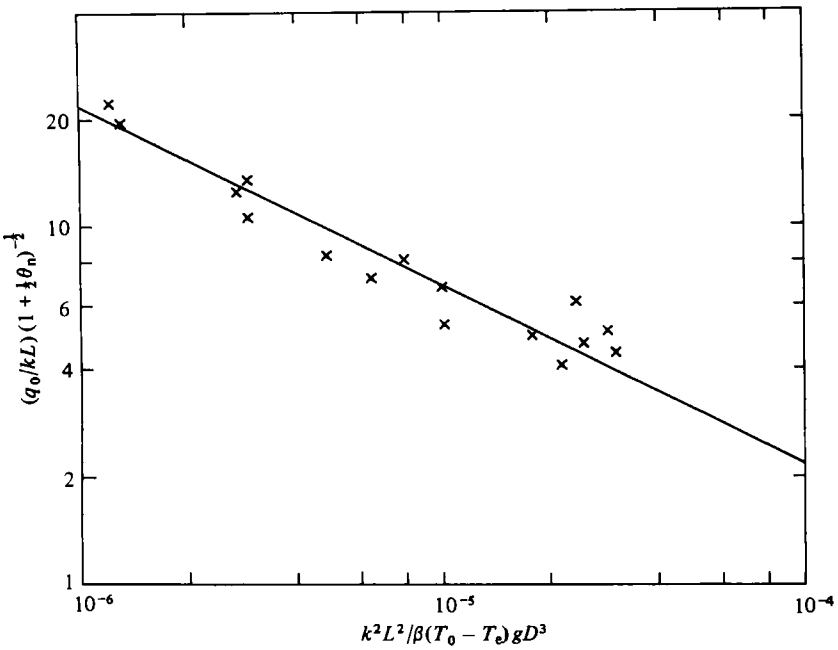

FIGURE 6. Comparison of (57) with the experimental data of Brocard *et al.* (1977).

The analytical results compare fairly satisfactorily with the experimental data. The scatter in the data can be explained by difficulties in the measurements of flow rates and estimation of surface buoyancy flux in the experiments, and the assumption regarding the length of the established flow region.

3.1. *Profile constants*

The constants $C_1, \ldots, C_5$ can be evaluated from the measured velocity and temperature profiles given by Sturm (1976). The velocity and temperature distributions of Sturm, after normalization, are shown in figure 7. The results of Sturm indicate a non-uniform temperature distribution in the upper layer, while the temperature data of Brocard *et al.* (1977) (who did not present velocity profiles) show a uniform temperature in this region, as one would expect in an unstable layer. The temperature profile of Sturm was therefore modified (figure 7) to evaluate the constants. The values of the constants for these profiles are: $C_1 = 0{\cdot}30$, $C_2 = 0{\cdot}37$, $C_4 = 0{\cdot}25$ and $C_5 = 0{\cdot}23$. It was found difficult to determine the value of C_3 (the velocity gradient at $\eta = 0$) accurately from the measured velocity profile of Sturm. The value of C_3 was therefore obtained from (14), which was integrated using the measured velocity and temperature data for run B of Sturm. The velocity distributions at $\xi = 40$ and $\xi = 80$ (not presented here) are almost identical, indicating an insignificant downflow in the reach considered; u_s is therefore a constant between these two sections.

Consequently, the contribution to the integral of the first term in (14) is zero. The value of C_3 was then determined by substituting the measured values of u_s and $T_s - T_n$ at $\xi = 40$ and 80 and D in (14), and was found to be 210. The value of the parameter δ_2 in (56) and (57) for these values of the profile constants and for a modified

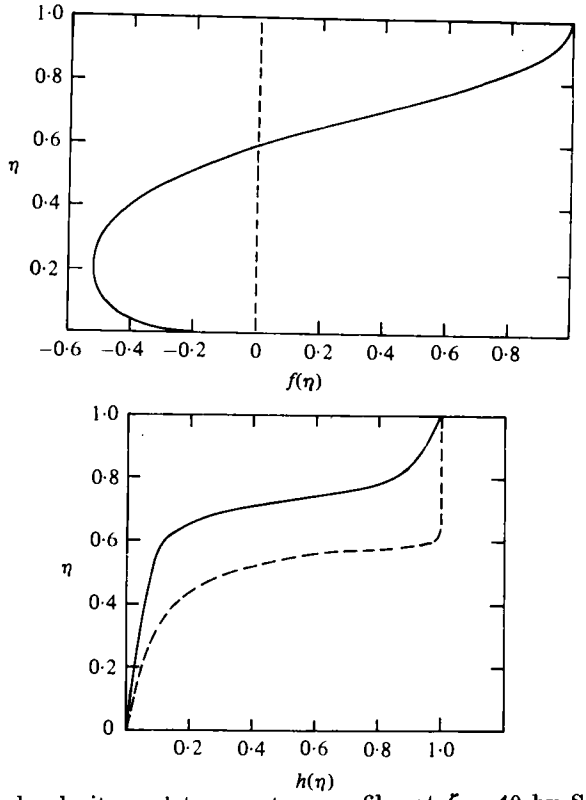

FIGURE 7. Measured velocity and temperature profiles at $\xi = 40$ by Sturm (——). Modified temperature profile (— — —).

Prandtl number P_m of 0·5 (which is the average value of P_m for the data plotted in figures 5 and 6) is 0·072, which is in a good agreement with the value of δ_2 of 0·067 and 0·071 determine from figures 5 and 6 respectively.

REFERENCES

AMES, W. F. 1968 *Nonlinear Ordinary Differential Equations in Transport Processes.* Academic.

BROCARD, D. N., JIRKA, G. H. & HARLEMAN, D. R. F. 1977 A model for the convective circulation in side arms of cooling lakes. *Ralph M. Parsons Lab. for Water Resources and Hydrodynamics, MIT, Rep.* no. 223.

BROCARD, D. N. & HARLEMAN, D. R. F. 1980 Two-layer model for shallow horizontal convective circulation. *J. Fluid Mech.* **100**, 129–146.

EDINGER, J. R. & GEYER, J. C. 1965 Cooling water studies for Edison Electric Institute. *The Johns Hopkins University, Project* RP-49: *Heat Exchange in the Environment.*

JAIN, S. C. 1980 Density currents in sidearms of cooling ponds. *Proc. A.S.C.E., Energy Div.* **106** (EY1), 9–21.

PHILLIPS, O. M. 1966 On turbulent convection currents and the circulation of the sea. *Deep-Sea Res.* **13**, 1149–1160.

RYAN, P. J., HARLEMAN, D. R. F. & STOLZENBACH, K. D. 1974 Surface heat loss from cooling ponds. *Water Resources Res.* **10**, 930–938.

STURM, T. W. 1976 An analytical and experimental investigation of density currents in sidearms of cooling ponds. Ph.D. thesis, Department of Mechanics and Hydraulics, University of Iowa.

STURM, T. W. & KENNEDY, J. F. 1980 Heat loss from sidearms of cooling lakes. *Proc. A.S.C.E. Hydraul. Div.* **106** (HY5), 783–804.